JOURNAL OF MATERIALS SCIENCE **36** (2001) 3759–3768

# Effect of the solvent on the particle morphology of spray dried PMMA

X. D. ZHOU, S. C. ZHANG, W. HUEBNER, P. D. OWNBY
*Department of Ceramic Engineering, University of Missouri-Rolla, Rolla MO 65409, USA*
HONGCHEN GU
*Institute of Technical Chemistry and Physics, East China University of Science and Technology, Shanghai, People's Republic of China 200237*
*E-mail: ownby@umr.edu*

The effect of various solvents on the morphology of polymethyl methacrylate (PMMA) particles synthesized by spray drying is examined. It is concluded that the product PMMA particles, derived from the PMMA-acetone dilute solution, have a smaller particle size than those from the PMMA-THF dilute solution. This is due to the stronger PMMA-acetone interaction, since acetone is a good solvent for PMMA, while THF is a poor solvent for PMMA. By controlling the temperature of each section of the tube furnace, the heating rate was adjusted so that both solid and hollow particles could be obtained. When water was added to these dilute solutions, porous or honeycomb particles were produced due to the different evaporation rates of solvent and water. This was a result of a large difference in the solubility parameter values between PMMA and solvent. The strong interaction between PMMA and acetone results in the formation of porous particles while the weak interaction between THF and PMMA produced honeycomb structure particles.


## 1. Introduction

Steady progress in developing commercially viable techniques to produce ultrafine powders (submicron) has been made since the early 1980's. Most studies have focused on inorganic materials, with only a few papers treating polymer particles [1–3]. This is somewhat surprising, since polymer particles are of great importance in a variety of areas including cosmetics, membrane coatings, films, pharmaceutical manufacturing, biomedical engineering, etc. Their use in these areas not only requires that the polymer particles be in the ultrafine state, but also that the particles have designed morphologies.

Several methods are commonly used for the synthesis of polymer particles, including bulk or suspension polymerization, mechanical comminution, and solution precipitation. The suspension polymerization method is not easily controlled, and has problems due to particle flocculation. The second method is strongly dependent on the physical properties of the primary pre-milled particles, and the resulting particles tend to be large ($\sim$10 $\mu$m). The particle morphology cannot be easily controlled by either of these methods. Ugelstad *et al*. [4] proposed a new method, activated swelling, to produce a number of different morphologies, including monosized spheres as well as porous particles. An emulsion method was used by Sjostrom *et al*. [5] to form organic particles by dissolving organic substances in a solvent, dispersing the solution in a non-solvent to form an emulsion, and then obtaining the organic particles after solvent evaporation. They found that the evaporation of the solvent was a rapid process with the rate determined by diffusion of the solvent out of the water suspension. The dry product particles still needed to be separated from the suspension.

Aerosol spray reactors were used to synthesize polymer particles by Matijevic *et al*. [1, 6] and Shin *et al*. [7]. Compared with bulk polymerization, there are several advantages to the aerosol synthesis of polymer particles: 1) the particle diameter can be controlled by changing the initial aerosol size, 2) no surfactants are needed, which results in a high chemical purity of the product particles, and 3) the process is easily controlled compared to bulk polymerization. However, since most polymer monomers have a high vapor pressure, the application is limited. Additionally, both the average molecular weight of the polymers and the particle morphology are difficult to change.

The effect of the solvent on ceramic particle morphology has been investigated [8–14] for materials such as titania and silica. Kaji *et al*. [8] studied the effect of different solvents on the morphology of gelling alkoxy-derived silica. They found that for ceramic particles synthesized through the liquid phase, chemical interactions of the solvents on the particle surface were important. Park *et al*. [9] used FTIR spectroscopy to investigate chemical interactions at the solvent-particle interface during the formation of $TiO_2$ from solvated $TiCl_4$. In this case the morphology of the precipitates was controlled by adjusting the volume ratio of

n-propanol to water. Zhang *et al*. [15] studied the morphology of ceramic particles formed by spray pyrolysis and proposed that both surface and volume precipitation during drying of the droplet controlled the morphology.

In the polymer field, the effects of different solvents on the crystalline morphology during the casting process has been widely studied. For instance, Asaletha *et al*. [10] found that the morphology of a binary polymer blend strongly depended on the nature of the casting solvent. They attributed the phenomenon to the difference in the solubility parameters of polymers in the solvents. However, few published papers focus on how the solvent affects polymer particle morphology during particle formation.

Foks *et al*. [11] found that both the evaporation rate and the crystallization temperature determine the morphology of spherulites. At a given temperature, they found that a fast evaporation rate leads to only one type of spherulite, while a slow evaporation rate yielded different types of spherulites. After analyzing the interfacial intermolecular interactions by Langmuir adsorption isotherms of polymethyl methacrylate (PMMA) onto polypyrrole (PPy) and by studying the chain conformation of adsorbed macromolecules, Abel *et al*. [12] determined the effect of the solvents $CHCl_3$ and tetrahydrofuran (THF) on PMMA coated PPy with films of 16 nm thickness. A powerful solvent effect was obtained for this relatively thin film. Similar research studying the effect of different solvents on cast-film morphology, was done by Wu *et al*. [13] and Browne *et al*. [14]. In a spray process, Leong [16] studied the droplet morphology after solvent evaporation, using both theoretical models and experimental data.

In this paper, PMMA particles were synthesized by the spray technique, which is akin to the aerosol technique of synthesizing particles. The effects of operating conditions and solvent choice on the particle morphology are reported.

## 2. Experimental procedure

### 2.1. Spray drying system

Fig. 1 is a schematic diagram of the spray drying system used in these studies. The dryer consists of three subsystems: 1) aerosol generation, 2) drying, and 3) particle collection.

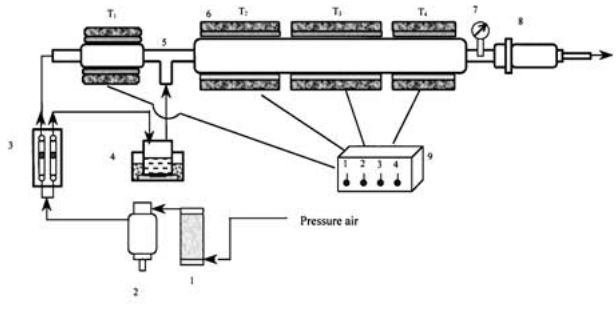


*Figure 1* Schematic of the experimental setup.

TABLE I Range of reactor operating conditions

| Parameter | | Range |
|---|---|---|
| Temperature | $T_1$ | 20–40° C |
| | $T_2$ | 20–60° C |
| | $T_3$ | 20–80° C |
| | $T_4$ | 80° C |
| Gas Flow Rate | Carrier Gas | 0.8 to 2 l/min |
| | Aerosol Gas | 0.8 to 5 l/min |

The aerosol was generated through ultrasonic nebulization (1.7 MHz, Ultra-Neb 99, DeVilbiss Co.) of various precursors. The size of the aerosol droplets is controlled by the frequency of the transducer, and the precursor characteristics.

The dryer is a horizontal refractory glass flow tube reactor (I.D. 54 mm, O.D. 60 mm, length 1.8 m), with a vacuum pump to maintain a negative pressure in the system. The temperature was controlled using heating tape wrapped around the tube, with four distinct temperature zones. Preheated or unpreheated air carrier gas was used to sweep the droplets, through a three-section furnace, with a set temperature in each section. The operating temperature ranges are shown in Table I, where the function of the fourth section was to prevent the solvent vapor from condensing.

The flow rate of the carrier air ranged from $2.77 \times 10^{-5}$ m$^3$/s to $1.38 \times 10^{-4}$ m$^3$/s. The corresponding residence time of carrier air in the heated zones was estimated to be from 30 s to 150 s. The temperature of each section of the furnace was controlled independently. Particles were collected with 1 $\mu$m filter paper supported by a cotton bag.

### 2.2. Polymer precursors

The raw PMMA used in this study had an average molecular weight of 120,000 (Aldrich Co.). Precursor solutions were prepared by dissolving the PMMA in various solvents. A Sigma 703 tensiometer (KSV Instruments Ltd.) and a Haake Vt500 viscometer (Mess-Technik, GmbHu Co.) were used to measure the surface tension and viscosity of the precursor solution, respectively.

### 2.3. Particle characterization

The morphology and size of the powders produced were evaluated with an SEM (Hitachi S-570 and JEOL T330A). The particle size distribution was analyzed from SEM images of over 300 individual particles using National Institute of Health (NIH) software.

## 3. Results and discussion

### 3.1. Theory

Acetone is a good solvent for PMMA [17], which means that the polymer-solvent interaction favors polymer-solvent contact over the polymer-polymer contact. Acetone is a thermodynamically favored solvent [18] and the Lewis base, THF, is a poor solvent [12] for the basic

polymer, [19] PMMA. Two types of interactions need to be considered in PMMA solutions; namely, Lewis acid-base interactions and van der Waals dispersion force interactions. Lewis acid-base interactions are described by Drago's constants, $E_B$ and $C_B$, representing electrostatic interaction, and covalent bonds, respectively. The van der Waals interactions are described by the solubility parameter, $\delta$, representing the attractive strength between molecules of the material. The solubility parameter has been defined as the square root of the cohesive energy density:

$$\delta_i = \left(\frac{\Delta E_i^V}{V_i}\right)^{\frac{1}{2}}$$

where the $\Delta E$ is from:

$$\Delta H_m = V\left(\left(\frac{\Delta E_1^V}{V_1}\right)^{1/2} - \left(\frac{\Delta E_2^V}{V_2}\right)^{1/2}\right)^2 \phi_1\phi_2$$
$$= \text{the Enthalpy of mixing}$$

where the subscript 1 represents the solute and 2 represents the solvent and $V =$ the molar volume.

The Gibbs free energy of mixing $= \Delta G_m = \Delta H_m - T\Delta S_m$ where $\Delta S_m$ is the Entropy of mixing and $T$ is the absolute temperature.

$\Delta G_m$ will always be less than zero for regular solutions if $\delta_1 = \delta_2$ and the components will be miscible in all proportions. Normally, the smaller the difference of the solubility parameter values, the easier the polymer dissolves. An acceptor number, AN, was used to correct the above interactions following Riddle and Fowkes [19], where the base solvent had a small AN value. The constants are shown in Table II. THF is much more basic than acetone, resulting in the weak interaction between PMMA-THF, since PMMA is a kind of basic polymer.

## 3.2. Solid particle formation

Peskin and Raco proposed [23] that the average droplet size ($d_d$) formed by ultrasonic atomization of liquid was

$$\frac{d_d}{\pi a} = \left[\left(\frac{2\sigma}{\rho f^2 a^3}\right) 2\tan h\left(\frac{\pi a}{d}\right)\left(\frac{h}{a}\right)\right]^{\frac{1}{3}}$$

where $d_d$ is the liquid droplet size, $h$ is the liquid film thickness, $\rho$ is the density of liquid, $\sigma$ is the surface tension, $a$ is the transducer amplitude and $f$ is the frequency. For large $h$, this equation can be written as:

$$d_d = 0.34\left(\frac{8\pi\sigma}{\rho f^2}\right)^{\frac{1}{3}}$$

Based on the mass conservation law, the theoretical diameter of the spray dried PMMA particles, $d_p$, derived from PMMA precursor with mass concentration, $C$, can be calculated from:

$$d_p = \sqrt[3]{\frac{C\rho_l}{\rho_p}} \cdot d_d$$

where $\rho_l$ is the precursor density, and $\rho_p$ is the PMMA theoretical density. Fig. 2 illustrates the possible mechanisms for particle formation with different morphologies. When a higher carrier gas temperature is used, the aerosol-synthesized particle size is larger than those produced at low temperature. This is because at high temperatures, rapid evaporation of the solvent and surface crystallization occurs, which results in hollow, larger particles. If the evaporation rate is slow, volume crystallization results, and the particles are mostly solid.

Fig. 3a and b are the SEM photomicrographs of PMMA particles derived from the precursors of 2.0 wt% PMMA in acetone and THF, respectively. The experimental parameters are listed in Table III. For the

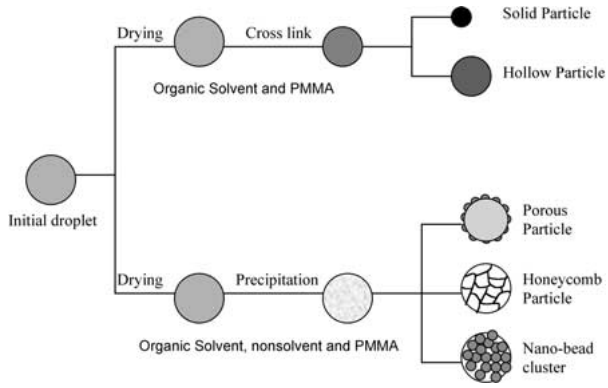


*Figure 2* Schematic of particle formation routes resulting in different morphologies.

TABLE III Properties and results of sample SP-11 and SP-13

| | Solvent | $T_1$°C | $T_2$°C | $C_{PMMA}$ (wt%) | $\sigma$ (mN/m) | $d_p$ ($\mu$m) |
|---|---|---|---|---|---|---|
| SP-11 | Acetone | 20 | 40 | 2.00 | 23.6 | 0.48 |
| SP-13 | THF | 20 | 40 | 2.00 | 26.6 | 0.68 |

TABLE II Constants of the raw materials

| | $E_B$ (kJ/mol)$^{1/2}$ | $C_B$ (kJ/mol)$^{1/2}$ | AN (kJ/mol) | $\delta$ (J/cm$^3$)$^{1/2}$ | Ref. |
|---|---|---|---|---|---|
| PMMA | 1.31 | 2.19 | | 19.1 | Abel [20], Brandrup[21] |
| THF | 2.00 | 8.74 | 2.09 | 18.6 | Riddle[19], Brandrup[21] |
| Acetone | 2.02 | 4.76 | 10.45 | 20.3 | Drago[22], Riddle[19], Brandrup[21] |
| Water | | | 63.11 | 47.9 | Riddle[19] Brandrup[21] |

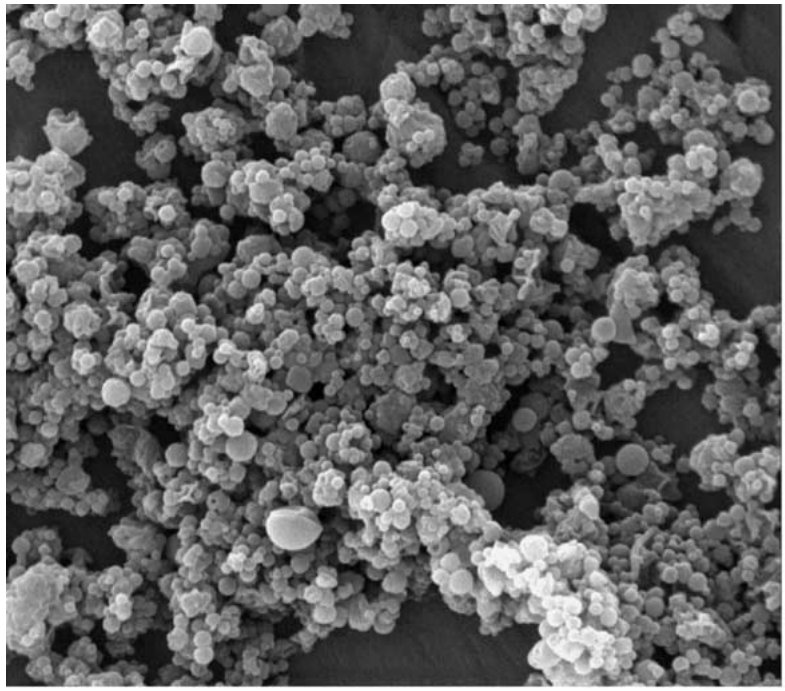

a

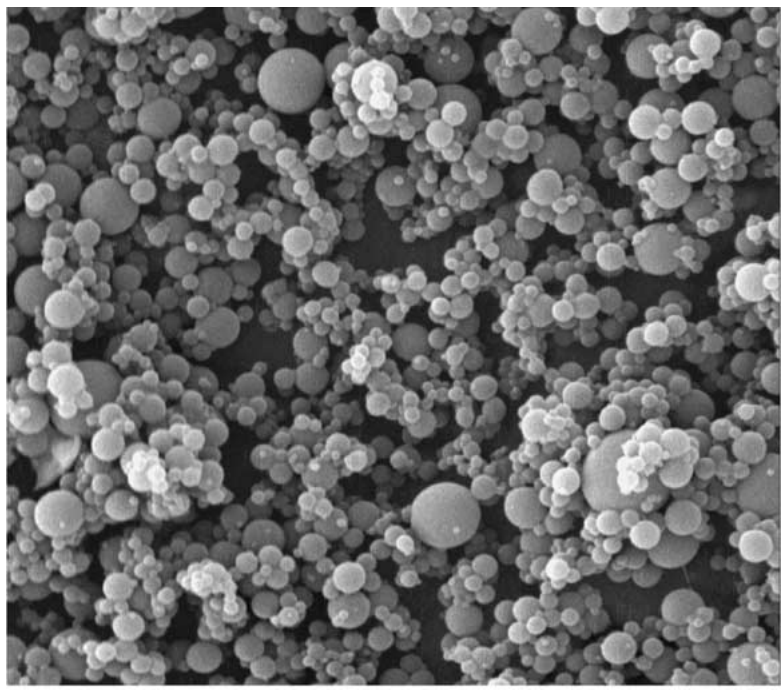


b

*Figure 3* SEM images of PMMA particles from slow heating.

acetone-PMMA solution with $\rho_l = 0.79 \times 10^3$ kg/m$^3$, $\rho_p = 1.18 \times 10^3$ kg/m$^3$, and $f = 1.7 \times 10^6$ Hz, the average liquid droplet size, $d_{d,} = 2.2$ $\mu$m and the average aerosol-synthesized particle size, $d_{p,} = 0.48$ $\mu$m.

The particle size distribution difference shown in Fig. 4 is related to the interaction characteristics of solvents with PMMA. Acetone evaporation resulted in an increasing PMMA concentration in the droplets followed by PMMA nucleation. This fact together with the strong PMMA-acetone interaction relative to the weaker interaction between PMMA polymer molecules, resulted in smaller particles. This phenomenon is similar to that of an inorganic species in aqueous solution, where the solute has a high solubility. On the other hand, THF solvent has a weak interaction with PMMA resulting in an early interaction of PMMA molecules, forming particles with larger average diameters.

### 3.3. Hollow particle formation

If a single anhydrous solvent, such as acetone, is used, the droplet-drying process of the precursor solution is

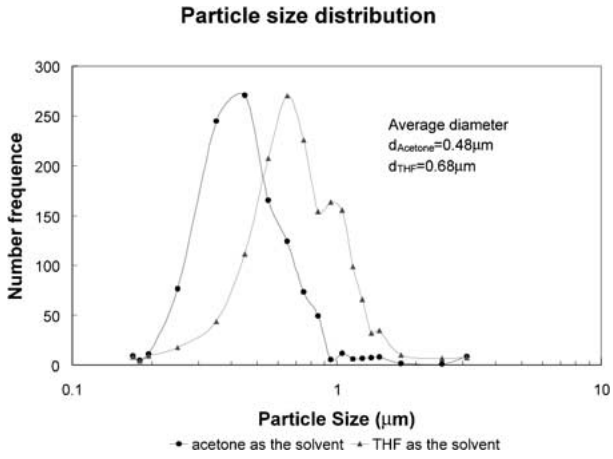


*Figure 4* PMMA particle size distribution, achieved from a single anhydrous solvent.

similar to that of an aqueous precursor droplet. According to the analysis in a previous paper [16], the heating rate is the key factor controlling the PMMA particle morphology. With a low temperature carrier gas ($T_1 = 20°C$), the heating rate in the second section has a significant effect on the particle morphology. If the temperature of the second section ($T_2$) is high, hollow PMMA particles are produced. When $T_2$ is low level, 40°C, solid particles are obtained, as shown in Fig. 3a. No effect of $T_2$ on the product particle morphology was observed with high carrier gas temperature ($T_1$).

If $T_2$ is high, the evaporation of acetone is rapid, and the PMMA molecules in the precursor droplet will "link" on the surface. When the PMMA molecules reach cross-link concentration on the droplet surface, the concentration at the droplet core is still below the cross-link concentration due since the rate of diffusion is slower than the rate of evaporation (shown in Fig. 5). When $T_2$ was increased to 70°C much larger hollow PMMA particles were obtained. The hollow particle formation mechanism is shown in Fig. 2.

Fig. 6a and b are SEM images of hollow PMMA particles obtained by rapid heating from acetone and THF, respectively. The particle size distributions of those samples are shown in Fig. 7. The mean particle diameter derived from the acetone solvent is still smaller than those from the THF solvent, however, the difference is less significant than when the particles are heated slowly as shown in Fig. 4. The operating conditions and results of these samples are shown in Table IV.

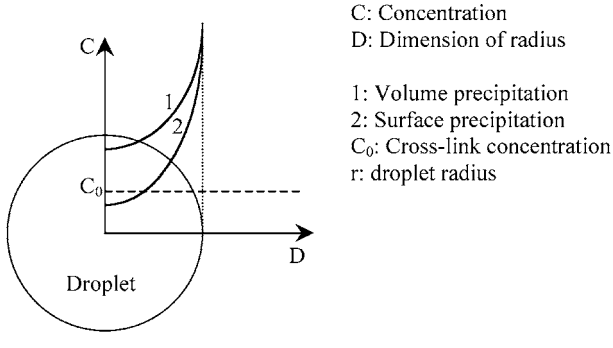


*Figure 5* Schematic of the droplet precipitation mechanism.

TABLE IV Properties of samples

| | Solvent | $T_1$°C | $T_2$°C | $C_{PMMA}$ (wt%) | $\sigma$ (mN/m) | $d_p$ ($\mu$m) |
|---|---|---|---|---|---|---|
| SP-30 | Acetone | 40 | 30 | 3.00 | 23.6 | 1.03 |
| SP-33 | Acetone | 40 | 40 | 1.00 | 23.6 | 1.35 |
| SP-34 | THF | 40 | 30 | 3.00 | 26.7 | 1.38 |
| SP-38 | Acetone | 40 | 50 | 1.00 | 23.6 | 1.31 |
| SP-50 | Acetone | 20 | 70 | 1.00 | 23.6 | |

Fig. 8a and b are the PMMA images obtained while $T_1 = 40°C$ and $T_2 = 40°C$ and 50°C respectively, as shown in Table IV. The size distribution is shown in Fig. 9. When the carrier gas was preheated, the effect of $T_2$ was not as significant on the PMMA particle morphology and size. For a single acetone droplet, the evaporation rate is:

$$\frac{dd_p}{dt} = f(d_p)\left(\frac{p_1}{T_1} - \frac{p_d}{T_d}\right)$$

where $f(d_p)$ is a function of the droplet diameter ($d_p$), and $T_1$ and $p_1$ are the temperature and vapor pressure in the ambient gas. $T_d$ and $p_d$ are the droplet surface temperature and the vapor pressure at the droplet surface. As $T_1$ increases, so does $T_d$. Since $p_1$ can be neglected, the ratio of $p_d/T_d$ will be much higher than $p_1/T_1$ at the high temperature, as shown in Fig. 10, resulting in the rapid evaporation.

## 3.4. Porous or honeycomb particle formation

### *3.4.1. Acetone-water*

When a single anhydrous organic solvent is used, the process of particle formation is similar to that of evaporation, drying, and gelation for an aqueous solution. However, if water is added to the acetone or THF base precursor solvents, the physical and chemical properties of the precursors will change, resulting in different PMMA particle morphologies and diameters. The solubility parameter $\delta_m$ of the mixed solvent is expressed by the rule of mixtures, $\delta_m = \delta_a\phi_a + \delta_b\phi_b$, where $\phi_a$, $\phi_b$ are the volume fraction of the two solvents. In these experiments, the weight ratios of acetone/water/PMMA was 89/10/1 corresponding to a mixed solvent content of 91 vol% acetone and 8 vol% water. The solubility parameter of the mixed solvent is $\delta_m = 22.6$, and the difference between it and solubility of PMMA, $\Delta\delta = \delta_m - \delta_{PMMA} = 22.6 - 19.1 = 3.5$, while that between acetone and PMMA was 1.2. With the acetone evaporation exceeding that of the water, the water fraction becomes larger and larger during the droplet drying process, resulting in a larger $\Delta\delta$. The evaporation rates of acetone and water were controlled by the operating conditions, and the $\Delta\delta$ value was changed by the volume ratio of acetone and water.

Fig. 11a–c are the SEM images of PMMA particles derived from the acetone-water solvent. The operating conditions and the particle characterization are shown in Table V. The particle size distributions of two of the samples are shown in Fig. 12. When the carrier gas was

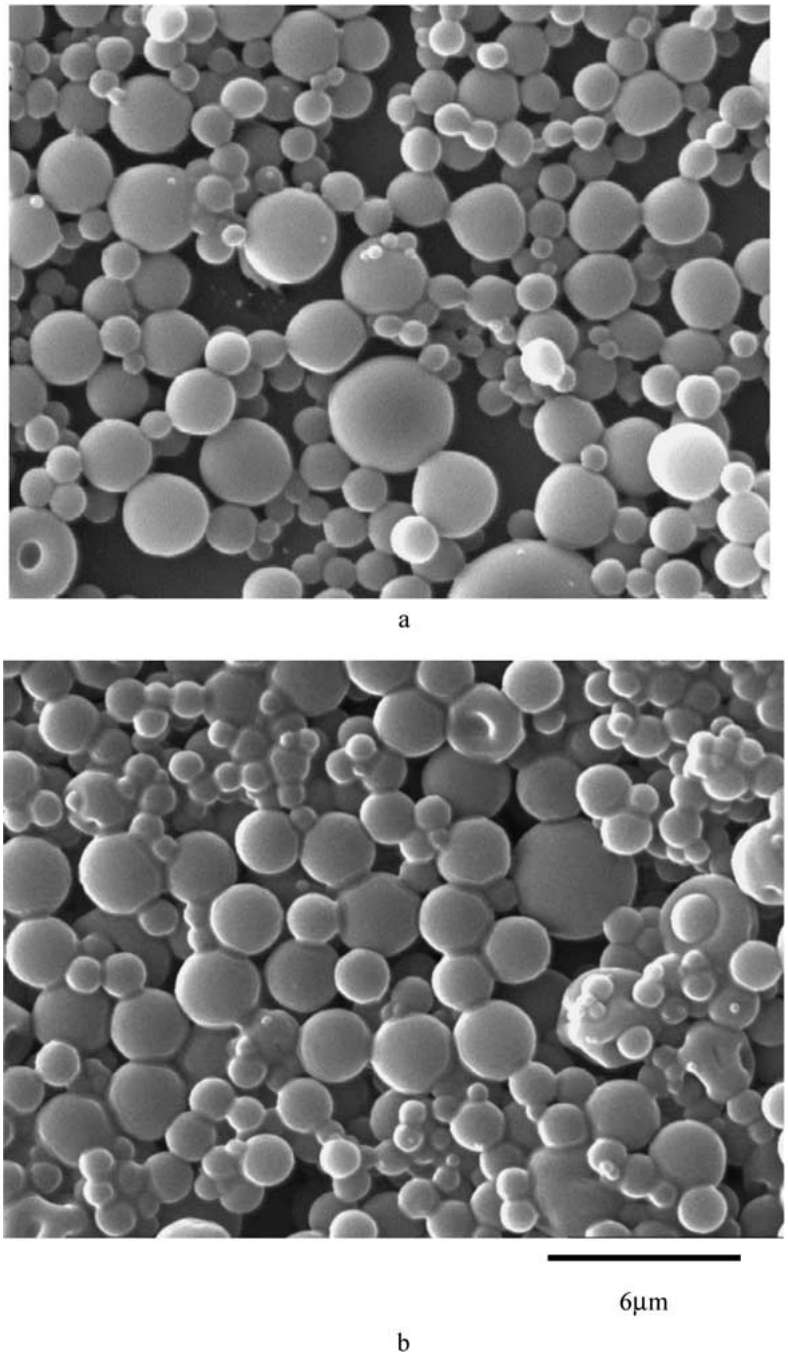


*Figure 6* SEM images of PMMA hollow particles from rapid heating.

TABLE V Properties and results of sample SP-27, SP-37 and SP-39

| | Solvent | $T_1$°C | $T_2$°C | $C_{PMMA}$ (wt%) | $\sigma$ (mN/m) | $d_p$ ($\mu$m) |
|---|---|---|---|---|---|---|
| SP-27 | Acetone-$H_2O$ | 20 | 30 | 1.00 | 25.8 | |
| SP-37 | Acetone-$H_2O$ | 20 | 50 | 1.00 | 25.8 | 2.22 |
| SP-39 | Acetone-$H_2O$ | 40 | 50 | 1.00 | 25.8 | 1.46 |

at room temperature and the temperatures of the second and third sections were kept at a low level (30°C), porous particles were obtained (Fig. 11a), and these porous particles consist of nano-scale particle clusters. When the temperature of the second section was increased to 50°C, the products were almost-all porous PMMA particles (Fig. 11b). A mixture of smooth and porous surface particles was obtained if the carrier gas was pre-heated (Fig. 11c).

In the situation shown in Fig. 11a, at the low temperature, the acetone evaporated more rapidly than water since $p_{acetone} = 30.8$ kPa, $p_{water} = 3.16$ kPa at 25°C [24], and then the PMMA-rich phase separated from the water phase because of the interaction of PMMA-acetone and the insolubility of PMMA in water. The rich-PMMA phase formed the nano-scale particles, and then the porous particles clustered after the water evaporated.

When the heating rate was high, the acetone evaporation and the phase separation rate were fast, resulting in a large amount of the porous PMMA particles as shown in Fig. 11b. At 50°C, $p_{acetone} = 82.0$ kPa, and $p_{water} = 12.3$ kPa. If the carrier gas was pre-heated, mixted particles with a porous morphology and a smooth surface were obtained as shown in Fig. 11c. When anhydrous acetone was used as the solvent for

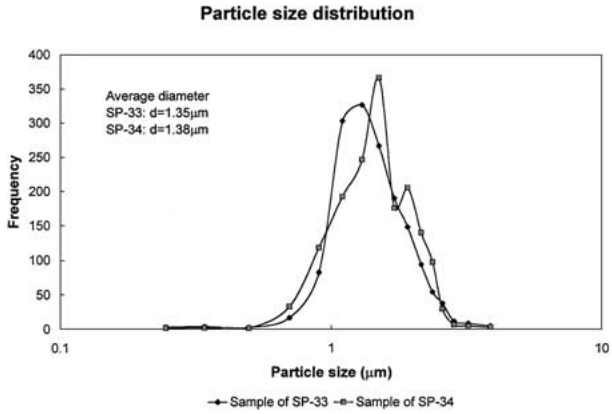


*Figure 7* Particle size distribution of samples SP-33 and SP-34.

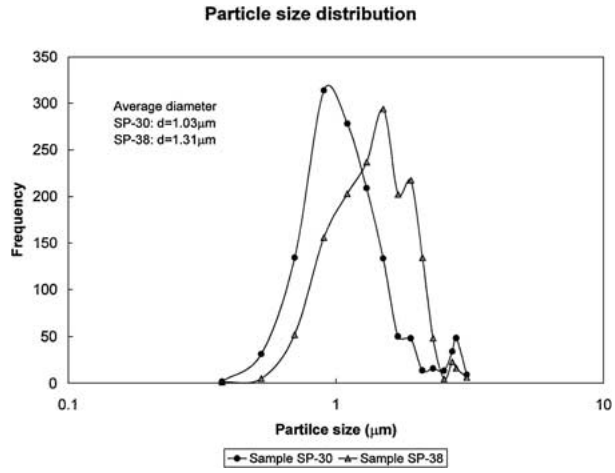


*Figure 9* Particle size distribution of samples SP-30 and SP-38.

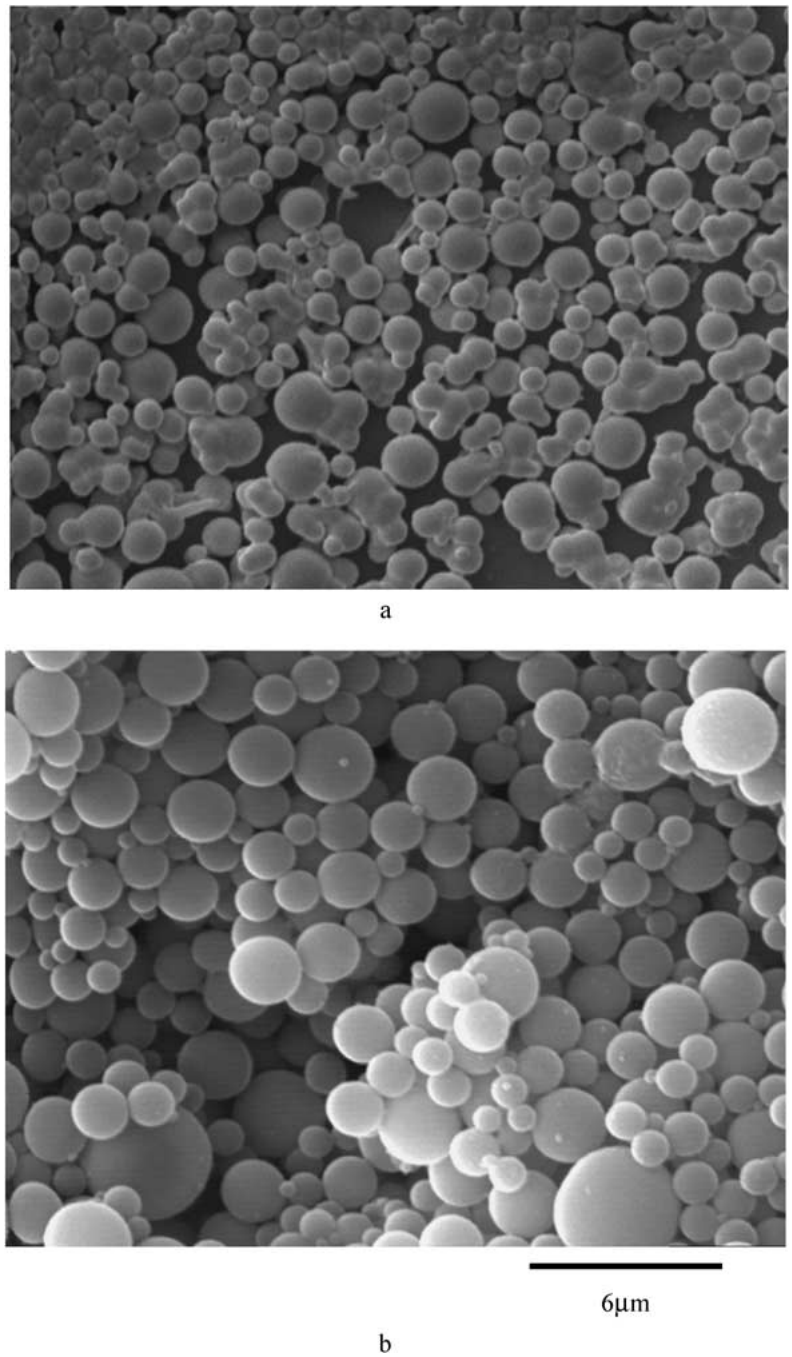


*Figure 8* SEM images of acetone derived PMMA particles at different heating rates.

PMMA, hollow particles were obtained with the same operating condition as that for sample SP-37 in Fig. 11b. The mechanism of porous particle formation is shown in Fig. 2.

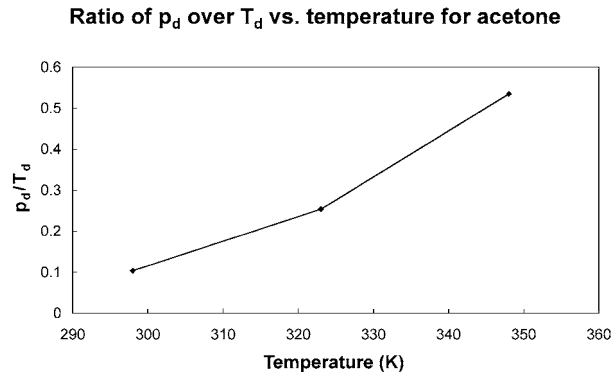


*Figure 10* Ratio of $p_d$ over $T_d$ vs. temperature for acetone.

### 3.4.2. THF-water

THF being basic and a poor solvent for the basic polymer PMMA, was found by Abel *et al*. [12, 20] to produce a roughening of a cast film whereas if a good solvent was used, no roughening occurred due to the strong solvent-polymer interactions.

In our experiments, when a THF/water system was used, the particle morphology was also different from those that resulted from the acetone/water solvent system. The interactions between THF and PMMA are weak but when water is added, the interactions are further decreased since water is a non-solvent and interacts with THF by hydrogen bonding. So linking of PMMA chains is enhanced in the THF/water-PMMA system. These chains cross-link and are segregated by the water phase. After the THF and water evaporates, these chains form a honeycomb structure. The honeycomb particle image is shown in Fig. 13. Fig. 2 shows the schematic

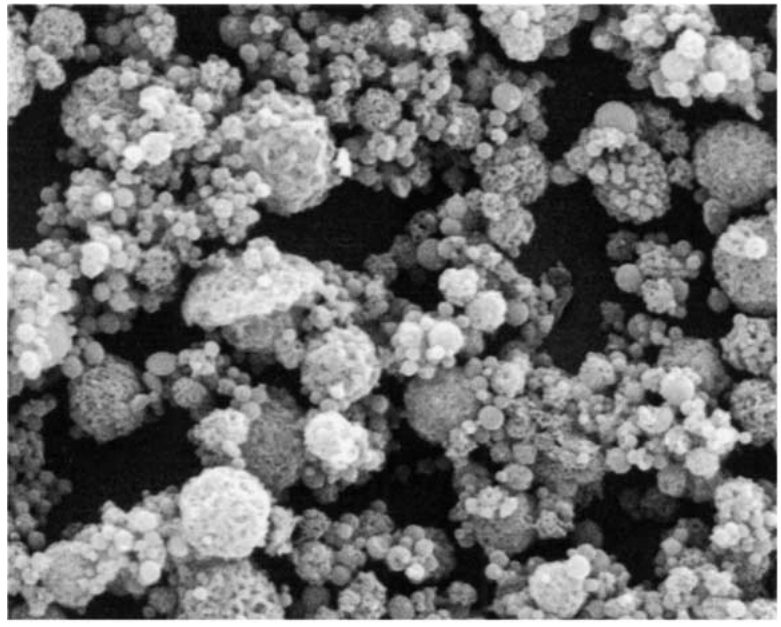

a

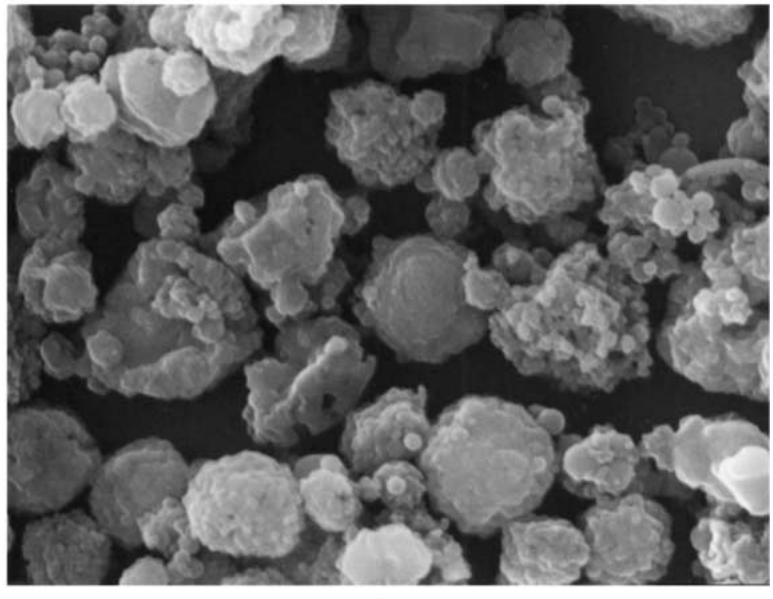

b

*Figure 11* SEM images of acetone/water derived PMMA particles *(Continued)*.

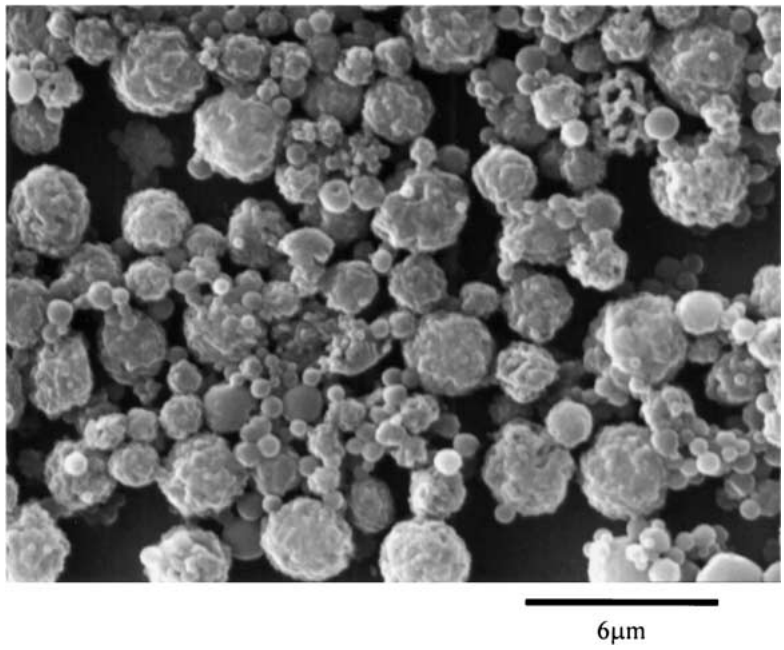


*Figure 11 (Continued).*

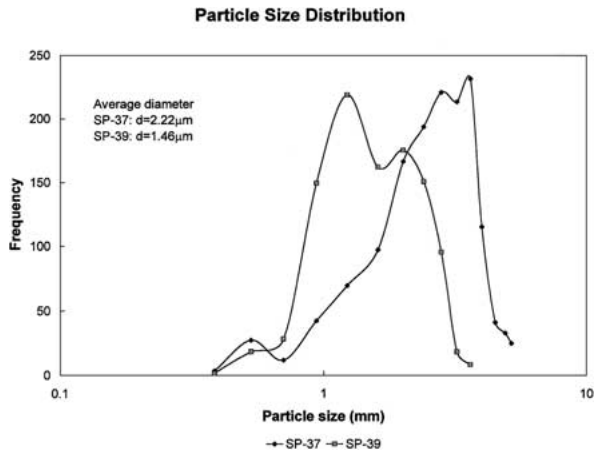


*Figure 12* Particle size distribution of samples SP-37 and SP-39.

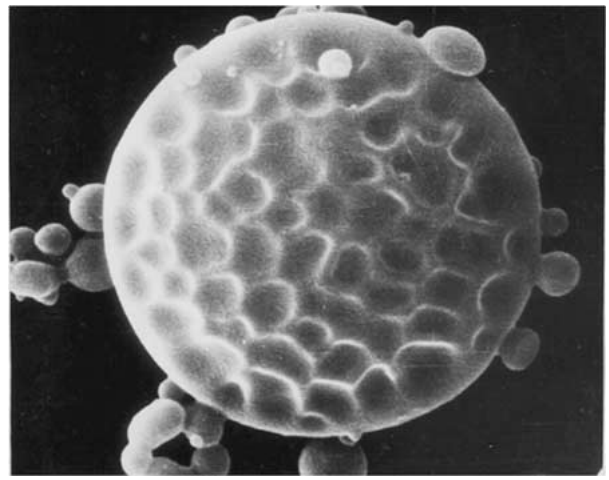

*Figure 14* SEM image of a golf ball shaped PMMA particle.

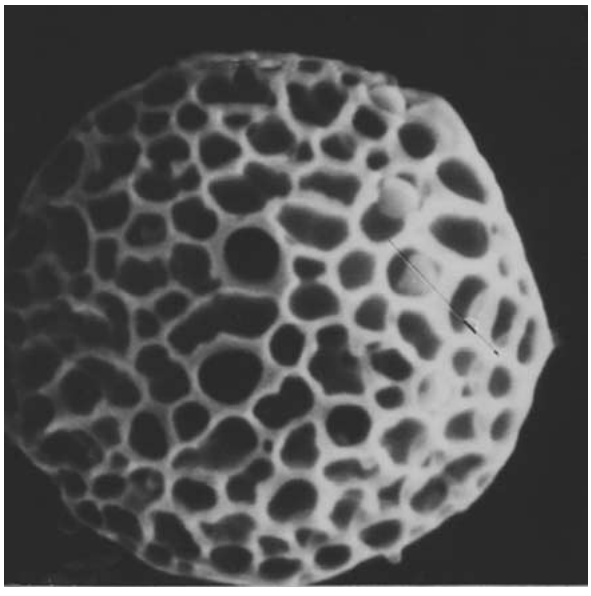

*Figure 13* SEM image of a honeycomb PMMA particle.

representation of the formation of the porous and the honeycomb particles.

If the temperature of the third section was high, closed pore, golf ball shaped particles were obtained due to edge-melting along the small pores as shown in Fig. 14.

## 4. Conclusions

Solid PMMA particles are produced when a single anhydrous solvent, either acetone or THF, is used under the low drying rate operating conditions. Since acetone is a good solvent for PMMA compared to the THF, the strong interaction of acetone and PMMA results in particles with a larger mean size than those from the THF-PMMA system. Hollow particles were obtained when the drying rate was high with no significant difference in the particle size between the two solvents.

When water was added to the organic solvents, the physical properties of the particles were changed due to a change in the solubility during the drying process. Porous particles were obtained from acetone/water-PMMA while honeycomb particles were obtained from THF/water-PMMA. Since acetone has a strong interaction with PMMA, nano PMMA beads were formed when PMMA precipitated from the solution. THF is a poor solvent for PMMA, resulting in a weak interaction of THF and PMMA, so that PMMA chains are formed. Linking of these chains segregated by the water phase resulted in honeycomb particles. These honeycomb particles can be further modified by increasing the temperature in the final stage of the synthesis process resulting in golf ball shaped particles.

## Acknowledgement

The authors acknowledge the support of this research by the University of Missouri Research Board.

## References

1. E. MATIJEVIC, *Ann. Rev. Mater. Sci.* **15** (1985) 483.
2. J. UGELSTAD, J. R. MFUTAKAMBA, P. C. MORK, T. ELLINGSEN, A. BERGE, R. SCHMID, L. HOLM, A. JORGEDAL, F. K. HANSEN and K. NUSTAD, *J. Polymer Science*, Polymer Symposia, 72 (John Wiley and Sons, New York, NY, USA, 1983) p. 225.
3. C. ESEN and G. SCHWEIGER, *Chem. Eng. and Tech.* **21**(1) (1998) 36.
4. J. UGELSTAD, A. BERGE, T. ELLINGSEN, R. SCHMID, T.-N. NILSEN, P. C. MORK, P. STENSTAD, E. HORNES and O. OLSVIK, *Prog. Polym. Sci (Oxford).* **17**(1) (1992) 87.
5. B. SJOSTROM, B. BERGENSTAHL, M. LINDBERG and A. C. RASMUSON, *J. Dispersion Science and Technology* **15**(1) (1994) 89.
6. R. E. PARTCH, K. NAKAMURA, K. J. WOLFE and E. MATIJEVIC, *J. Colloid Interface Science* **105** (1985) 560; K. NAKAMURA, R. E. PARTCH and E. MATIJEVIC, *ibid.* **99**(1) (1984) 118; C. J. ZIMMERMANN, R. E. PARTCH and E. MATIJEVIC, *J. Aerosol Science* **22**(7) (1991) 881.
7. D. S. SHIN, E. K. OH and S.-G. KIM, *Aerosol Science and Technology* **24**(4) (1996) 243.
8. H. KAJI, K. NAKANISHI and N. SOGA, *J. Non-Cryst. Solids* **181**(1-2) (1995) 16.
9. H. K. PARK, D. K. KIM and C. H. KIM, *J. Amer. Ceram. Soc.* **80**(3) (1997) 743.
10. R. ASALETHA and M. G. KUMARAN, *Polym.-Plast. Technol. Eng.* **34**(4) (1995) 633.
11. J. FOKS and M. LUSZCZEK, *J. Cryst. Growth* **134** (1993) 347.
12. M. L. ABEL, J. L. CAMALET, M M. CHEHIMI, J. F. WATTS and P. A. ZHDAN, *Synthetic Metals* **81** (1996) 23.
13. W. B. WU, W. Y. CHIU and W. B. LIAU, *J. Appl. Polym. Sci.* **6**(3) (1997) 411.
14. M. M. BROWNE, M. FORSYTH and A. A. GOODWIN, *Polymer* **38**(6) (1997) 1285.
15. S. C. ZHANG and G. L. MESSING, *J. Amer. Ceram. Soc.* **73**(1) (1990) 61; G. L. MESSING, S. C. ZHANG and G.V. JAVANTHI, *ibid.* **76**(11) (1993) 2707.
16. K. H. LEONG, *J. Aerosol Sci.* **12**(5) (1981) 417; *Idem., ibid.* **18**(5) (1987) 525.
17. H. FUJITA, "Polymer Solutions" (Elsevier Science Publishers, B V, 1990).
18. C. KONAK, M. HELMSTEDT and R. BANSIL, *Macromolecules* **30** (1997) 4342.
19. F. M. FOWKES and M. A. MOSTAFA, *Ind. Eng. Chem. Prod. Res.* **17**(1) (1978) 3; F. L. RIDDLE JR and F. M. FOWKES, *J. American Chemical Society* **112**(9) (1990) 3529.
20. M. M. CHEHIMI, M. L. ABEL and S. ZOUBIDA, *J. Adhesion Sci. Technol.* **10**(4) (1996) 287.
21. J. BRANDRUP and E. H. IMMERGUT, "Polymer Handbook," 3rd edn. (John Wiley and Sons, 1989).
22. R. S. DRAGO, G. C. VOGEL and T. E. NEEDHAM, *Journal of the American Chemical Society* **93**(23) (1971) 6014.
23. R. L. PESKIN and R. J. RACO, *J. Acoustical Society of America* **35**(9) (1963) 1378.
24. D. R. LIDES and J. P. R. FREDERIKSE, "Handbook of Chemistry and Physics," 76th edn. (CRC Press, 1996).
25. T. ALLEN, "Particle Size Measurement," 4th edn. (Chapman and Hall, 1990).

*Received 28 February*
*and accepted 4 October 2000*